

Dissecting Person Re-identification from the Viewpoint of Viewpoint

Xiaoxiao Sun Liang Zheng
Australian National University

xxsunzrt@gmail.com liang.zheng@anu.edu.au

Abstract

Variations in visual factors such as viewpoint, pose, illumination and background, are usually viewed as important challenges in person re-identification (re-ID). In spite of acknowledging these factors to be influential, quantitative studies on how they affect a re-ID system are still lacking. To derive insights in this scientific campaign, this paper makes an early attempt in studying a particular factor, viewpoint. We narrow the viewpoint problem down to the pedestrian rotation angle to obtain focused conclusions. In this regard, this paper makes two contributions to the community. First, we introduce a large-scale synthetic data engine, PersonX. Composed of hand-crafted 3D person models, the salient characteristic of this engine is “controllable”. That is, we are able to synthesize pedestrians by setting the visual variables to arbitrary values. Second, on the 3D data engine, we quantitatively analyze the influence of pedestrian rotation angle on re-ID accuracy. Comprehensively, the person rotation angles are precisely customized from 0° to 360° , allowing us to investigate its effect on the training, query, and gallery sets. Extensive experiment helps us have a deeper understanding of the fundamental problems in person re-ID. Our research also provides useful insights for dataset building and future practical usage, e.g., a person of a side view makes a better query.

1. Introduction

Viewpoint, pose, illumination, background and resolution are a few visual factors that are generally considered as influential problems in person re-identification (re-ID). Currently, major endeavor is devoted to algorithm design to mitigate their impact on the system. Therefore, despite qualitatively acknowledging the factors as influential, it remains largely unknown how these factors affect the performance quantitatively.

In this paper, we study one of the most important factors, *i.e.*, viewpoint. Here, we denote viewpoint as the pedestrian rotation angle (Fig. 1). In what follows, we use viewpoint to replace pedestrian rotation angle unless specified. Since dif-

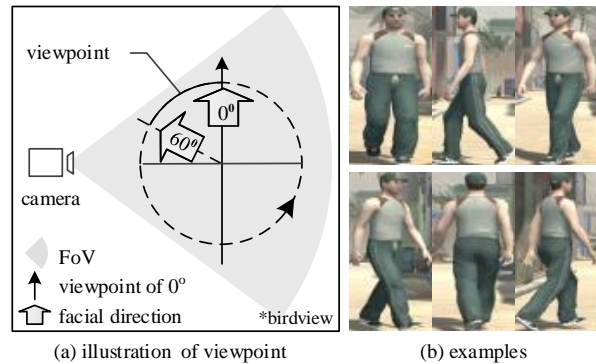


Figure 1. (a) Illustration of viewpoint of the birdview. Viewpoint is defined as the rotation angle of a person relative to a manually defined degree of 0° . The field of view (FoV) of a camera is shown. (b) Examples of persons under different viewpoints.

ferent views of a person contain different details, the viewpoint of a person influences the underlying visual data of an image, and thus the learning algorithm. Therefore, we aim to investigate the exact influence of viewpoint on the system. This study will benefit the community from two aspects. (1) The conclusions of this research can guide for building the training set effectively. For example, finding that certain angles are more important for learning models of identifying pedestrians. (2) It will advise for designing of query and gallery sets. By discovering viewpoints that are effective for re-ID accuracy, our research can potentially benefit the practical usage of re-ID systems.

In our attempt to reveal the influence of viewpoint, a notable obstacle is the lack of data. Existing datasets might have a biased and fixed distribution of environmental factors. In pedestrian viewpoint, for example, some angles might only have a few or even zero samples. In another example, when studying illumination on a real-world dataset, conclusions are less convincing because the dataset might only have a specific illumination condition. Further, a fixed/static data distribution forbids us from exploring how the impact of viewpoint relates to other visual factors. For example, the impact of viewpoint could be conditioned on the background, because background also affects feature learning. To fully understand the role of viewpoint, we need to test its influence by changing the environment to either

hard or easy modes. As such, without comprehensive and flexible data streams, we cannot make quantitative and scientific judgment of a visual factor’s significance.

This paper makes two contributions to the community. First, we build a large-scale data synthesis engine named PersonX. PersonX contains 1,266 manually designed identities and editable visual variables. It can simulate persons under various conditions. First of all, we demonstrate that existing re-ID models has **consistent accuracy trend** on both PersonX and real-world datasets [30, 31]. This observation suggests that **PersonX is indicative of the real world**. Moreover, as the name implies, the feature of PersonX is “controllable”. Persons take controllable poses and viewpoints, and the environment is controlled *w.r.t* the illumination, background, *etc.* Persons move by running, walking *etc.*, under the controlled camera view and scene. We can obtain the exact person bounding boxes without external detection tools and thus avoid the influence of detection errors on the system. Therefore, PersonX is indicative, flexible and extendable. It supports future research in not only algorithm design, but also scientific discoveries how environmental factors affect the system.

Second, we dissect a person re-ID system by quantitatively understanding the role of person viewpoint. Three questions are considered. (1) How does the *viewpoint of the training set* influence the system? (2) How does the query viewpoint influence the retrieval? (3) How does the re-ID accuracy change under different *viewpoint distributions of the testing set*? To answer these questions, we perform rigorous quantification on pedestrian images regarding viewpoints. We customize the viewpoints of persons in the PersonX engine from 0° to 360°. Both the control group and the experimental group are designed, so as to obtain convincing scientific conclusions. We also empirically study the real-world Market-1203 dataset where viewpoints of person are manually labeled. The empirical results are consistent with our findings on the synthetic data.

2. Related Work

We first review re-ID methods that improve the robustness against variations in pose, illumination, and background. We then review methods based on synthetic data.

Against pose variance. Some works [7, 29, 6, 21, 19] learn pose invariant representations for persons. For example, Farenza *et al.* [7] utilizes body symmetry on the x-axis and asymmetry on the y-axis two axes to design a descriptor with pose invariance. Cho *et al.* [6] quantize person poses into one of four canonical directions (front, right, back, left) to facilitate feature learning. Zheng *et al.* [29] design the PoseBox to align different persons along the body parts.

Against background variance. Some works reduce the influence of background [4, 26, 5, 20, 23]. For instance, Chen *et al.* [5] fuse the descriptors from the foreground per-

son and the original image, such that the foreground is paid more attention to by the network. In [20], Song *et al.* use binary segmentation masks to separate foreground from the background. They then learn representations from the foreground and background regions, respectively.

Against resolution variance. Resolution denotes the level of information granularity of an image. High resolution is typically preferred. But usually the resolution level differs significantly across images. It thus affects the effectiveness of the learned features. To solve this problem, Jing *et al.* [11] design a mapping function that converts the features of low-resolution images into discriminative high-resolution features. Li [15] *et al.* investigate a joint multi-scale learning framework to obtain a shared subspace across different scales, targeting at cross-scale image domain alignment. In [24], features from the bottom and top layers are concatenated during training and testing. Supervision signals are incorporated at each layer to train the multi-resolution features.

Against viewpoint variance. Learning viewpoint invariance is another focus [9, 25, 2, 12, 27]. For example, Both [9][12] regard viewpoint variations as the most prominent problem. In this area, Gray *et al.* [9] investigate the properties of localized features, while Karanam *et al.* [12] propose to learn dictionaries that can match person images captured under different viewpoints.

Learning from synthetic data. Leveraging synthetic data is a useful idea to alleviate the reliance on large-scale datasets. This strategy has been applied in problems like semantic segmentation [18], object tracking [8], traffic vision research [14] *etc.* In the person re-ID domain, SOMAset [3] is a synthetic dataset with 50 person models and 11 types of outfits. Barbosa *et al.* use SOMAset for training and test on real-world datasets. The accuracy was competitive. Bak *et al.* [1] also introduce a synthetic dataset SyRI including 100 characters. This dataset is featured by rich lighting conditions. A domain adaptation method is designed based on this dataset to fit real-world illumination distributions. Departing significantly from previous objectives of using synthetic dataset, this paper lays emphasis on quantitatively analyzing how visual factors influence the re-ID system. We derive useful insights by precisely controlling the simulator. This is a very early attempt of this kind in the community.

3. PersonX: A Controllable Person Engine

3.1. Description

Software. The PersonX engine¹ is built on Unity [16]. We create a 3D controllable world containing 1,266 person models. As a controllable system, it can satisfy various data requirements. In PersonX, the characters and objects look

¹The PersonX data engine, including pedestrian models, scene assets, project and script files *etc.*, are released at [link](#).



Figure 2. The PersonX dataset. (a): Background. In each background, a person can face toward a manually denoted direction, thus generating a controlled viewpoint. (1) - (3) represent backgrounds with uniform colors and (4) - (6) use street scenes as the background. (b): Sample pedestrians bounding boxes in background (4). Various persons wearing various clothes are shown.

realistic, because the texture and materials of these models are mapped from the real world by scanning real people and objects. The values of visual variables, *e.g.*, illumination, scenery and background, are designed to be editable. Therefore, PersonX is highly flexible and extendable.

Identities. PersonX has 1,266 hand-crafted identities including 547 females and 719 males. To ensure diversity, we hand-crafted the human models with different skin colors, ages, body forms (height and weight), hair styles, *etc.* The clothes of these identities include jeans, pants, shorts, slacks, skirts, T-shirts, dress shirts, maxiskirt, *etc.*, and some of these identities have a backpack, shoulder bag, glasses or hat. The materials of the clothes (color and texture) are mapped from images of real-world clothes. The motion of these characters can be walking, running, idling (standing), having a dialogue *etc.* Therefore, the 3D models in PersonX look realistic. Figure 2 (b) presents examples of identities of various ages, clothes, body shapes and poses.

3.2. Visual Factors in PersonX

PersonX is featured by editable environmental factors such as illumination, cameras, backgrounds and viewpoints. Details of these factors are described below.

Illumination. Illumination can be directional light (sunlight), point light, spotlight, area light, *etc.* Parameters like color and intensity can be modified for each illumination type. By editing the values of these terms, various kinds of illumination environment can be created.

Camera and scene. The configuration of cameras in PersonX is subject to different values of image resolution, projection, focal length, and height.

Background. Currently PersonX has six different backgrounds (Fig. 2). In each experiment we set 2-3 different backgrounds/cameras views. In each background/camera view, a person moves freely in arbitrary direction, exhibiting arbitrary viewpoints relative to the camera. In Fig. 2, backgrounds (4), (5) and (6) depict different street scenes. Among the three scenes, backgrounds (4) and (5) share the same illumination and ground color, while background (6)



Figure 3. Images of the same person with different viewpoint. Viewpoints of one identity are sampled at an interval of 10 degrees. Left represents the set of the viewpoints that contains more information on the left side of the person, *i.e.*, 320° - 40°. Similarly, other sides of the pedestrian are represented by front (50° - 130°), right (140° - 220°) and back (230° - 300°). The blue tags of viewpoint represents the due left, front, right and back of person, *e.g.*, 0° is the left viewpoint of person.

is a shadowed region and the ground color is gray. Meanwhile, backgrounds (1), (2) and (3) are pure colors and are used when background influence needs to be eliminated. Because we simplify our system into two cameras, we use various combinations of these six cameras to create different re-ID environments. When not specified, all the cameras have a high resolution of 1024×768.

Viewpoint. Figure 3 presents some image examples under specified viewpoints. Those images are sampled during normal walking. Specifically, a person image is sampled every 10° from 0° to 350° (36 different angles in total). Each angle has 1 image, so each person has 36 images. The entire PersonX engine thus has 36 (angles) × 1,266 (identities) ×

dataset		#identity	#box	#cam.	view
real data	Market-1501 [30]	1,501	32,668	6	N
	Market-1203 [30]	1,203	8,569	2	Y
	MARS [28]	1,261	1,191,003	6	N
	CUHK03 [13]	1,467	14,096	2	N
	Duke [17]	1,404	36,411	8	N
synthetic data	SOMAsset [3]	50	100,000	250	N
	SyRI [1]	100	1,680,000	–	N
	PersonX	1,266	273,456	6	Y
	PersonX _{123,456}	1,266	136,728	3	Y
	PersonX _{12,13}	1,266	91,152	2	Y
	PersonX _{45,46}	1,266	91,152	2	Y

Table 1. Comparison of real-world and synthetic re-ID datasets. “View” denotes whether the dataset has viewpoint labels.

6 (cameras) = 273,456 images.

For each person, the 36 images are divided into 4 groups, representing four orientations: left, front, right and back. We use “left” and “due left” to represent images from 320° to 40° , the image of 0° , respectively. This convention applies for other orientations.

Comparisons of PersonX and some existing re-ID datasets are presented in Table 1. There are two existing synthetic datasets, SyRI [1] and SOMAsset [3]. SyRI is used as an alternative data source for domain adaptation and does not have the concept of cameras. SOMAsset contains 250 cameras, which are uniformly distributed along a hemisphere around each person. Neither datasets are freely editable by the public. In comparison, PersonX has configurable backgrounds and much more identities. Importantly, it can be edited/extended not only for this study, but also for future research in this area.

4. Benchmarking and Dataset Validation

In this section, we aim to validate that PersonX is indicative of the real world, such that conclusions derived from this dataset can be of value to practice.

4.1. Methods and Subsets

We use IDE+ [32], triplet feature [10] and PCB [22] for our purpose. IDE+ is implemented on ResNet50. During training, the batch size is set to 64 and the model is trained for 50 epochs. The learning rate is initialized to 0.1 and decays to 0.01 after 40 epochs. The model parameters are initialized with the model pre-trained on ImageNet. For triplet feature, the number of identities per batch is set to 32 and number of images per identity is set to 4. So the batch size is $32 \times 4 = 128$. The learning rate is initialized to 2×10^{-4} and decays after 150 epochs (300 epochs in total). Training of PCB follows the standard setup described in [22].

Through combinations of the six backgrounds described in Section 3.2, PersonX has the following subsets.

- PersonX₁₂. It has backgrounds (1) and (2). Both are pure color backgrounds; the colors are similar.

#	method	IDE+		triplet feature		PCB	
		mAP	R1	mAP	R1	mAP	R1
1	Market-1501	67.3	86.5	68.1	85.6	77.4	92.3
2	Market-1203	66.7	71.0	72.8	75.6	77.8	81.4
3	DukeMTMC-reID	55.1	74.2	57.9	76.3	66.1	81.7
4	PersonX ₁₂₃	94.5	99.2	95.3	98.6	97.9	99.6
5	PersonX ₁₂	94.8	99.5	95.6	99.0	97.8	99.6
6	PersonX ₁₃	94.6	99.1	94.6	98.6	97.6	99.4
7	PersonX ₄₅₆	92.7	98.5	94.3	98.5	97.8	99.7
8	PersonX ₄₅	94.0	99.4	95.0	99.1	97.7	99.8
9	PersonX ₄₆	91.5	96.3	92.8	97.0	96.8	99.2
10	PersonX _{456-lr}	87.9	96.7	89.8	95.6	94.9	98.4
11	PersonX _{45-lr}	90.2	98.4	90.9	97.5	95.1	98.9
12	PersonX _{46-lr}	85.9	94.3	86.2	93.2	92.6	96.6

Table 2. Benchmarking the subsets of PersonX. We use mAP (%) and rank-1 (R1, %) accuracy for measurement. “lr” means the frames are low resolution of 512×242 instead of the original resolution 1024×768 . As detailed in the text, this table validates the eligibility, purity and sensitivity of PersonX.

- PersonX₁₃. The two cameras face backgrounds (1) and (3). The color difference between the two backgrounds is significant than that in PersonX₁₂.
- PersonX₁₂₃. This is a three-camera system, comprising backgrounds (1), (2) and (3).
- PersonX₄₅. It contains backgrounds (4) and (5) of street scenes. The two backgrounds are close in scene and illumination.
- PersonX₄₆. It consists of backgrounds (4) and (6). The two backgrounds have larger disparity than PersonX₄₅.
- PersonX₄₅₆. It is a three-camera system consisting of backgrounds (4), (5) (6).

Overall, PersonX₁₂, PersonX₁₃ and PersonX₁₂₃ are simple subsets, while PersonX₄₅, PersonX₄₆ and PersonX₄₅₆ are more complex ones. Moreover, we introduce low-resolution subsets to create more challenging settings. Here, we edit the image resolution of PersonX₄₅, PersonX₄₆ and PersonX₄₅₆ from 1024×768 to 512×242 . We use “-lr” to represent these low-resolution subsets.

For benchmarking, we randomly sample 410 identities for training and the rest 856 identities for testing. In each camera, an identity has 36 images (*i.e.*, 36 viewpoints), from which one image is selected as the query during testing. Therefore, the three-camera subsets, *i.e.*, PersonX₄₅₆ and PersonX₁₂₃, contain 44,280 ($410 \times 36 \times 3$) training and 92,448 ($856 \times 36 \times 3$) testing images. The two-camera subsets have 29,520 ($410 \times 36 \times 2$) training and 61,632 ($856 \times 36 \times 2$) testing images.

4.2. System Validation

We evaluate the three algorithms on both real-world and synthetic datasets. We use the standard evaluation protocols

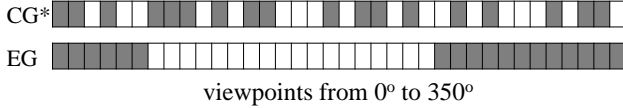


Figure 4. Design of the control group* (CG*) and experimental group (EG) when removing 1/2 of viewpoints. CG* means the training set contain 1/2 of viewpoints, *i.e.*, 18 viewpoints (white), that are randomly knocked out from 0°-350°. EG denotes 18 continuous viewpoints (white) are deleted.

[30, 31]. Results are reported in Table 2. We observe three characteristics of PersonX.

First, **eligibility**. We find the performance trend of the three algorithms is similar between PersonX and real-world datasets. On Market-1501 and DukeMTMC, for example, PCB has the best accuracy, and the performance of IDE+ and triplet feature is close. That is, $PCB \succ triplet \approx IDE+$. This is consistent with findings in [22]. On the synthetic PersonX subsets, the performance trend is similar: IDE+ and triplet feature have similar accuracy; PCB is usually 2%-3% higher than them. These observations suggest that PersonX is indicative of the real-world and that future conclusions derived from PersonX can be of real-world value.

Second, **purity**. The accuracy on PersonX subsets (#4 - #9) are relatively high. It does not mean these subsets are “easy”. In fact, the high accuracy is what we want, as it excludes the influence of the environmental factors. In other words, these subsets are “oracle”: images are high-resolution, and the scenes have normal sunlight and relatively consistent backgrounds. These subsets are thus ideal ones to study the viewpoints.

Third, **sensitivity**. We show that these subsets are sensitive to the changes in the environment. For example, background variation in PersonX₄₆ is much larger than PersonX₄₅. As such, we observe that mAP in PersonX₄₆ is lower by 1%-3%. Similarly, the background in PersonX₁₂ is much simpler than PersonX₄₆. The complex background causes rank-1 accuracy in PersonX₄₆ to be lower by 3%. Further, when these subsets are manually edited to be low resolution (“-lr”), we observe a significant mAP drop. For example, the mAP drop from PersonX₄₆ to PersonX₄₆-lr is 6%. The above comparisons demonstrate that PersonX subsets are sensitive to background complexity, background variation between cameras, and image resolution. This is consistent with our intuition and indicates that PersonX is useful in studying the influence of visual factors.

The above discussions indicate that PersonX is indicative of the real-world trend, has strictly controlled environment variables, and is reasonably sensitive to environmental changes. We believe PersonX will be a useful tool for the community and encourage development of robust algorithms and scientific analysis.

5. Evaluation of Viewpoint

We evaluate the impact of viewpoint on person re-ID. The experiment is based on PCB [22]. We note that other standard re-ID methods (*e.g.*, IDE+) can draw similar conclusions. Three questions will be investigated: how does the viewpoint in (1) the training set, (2) the query set, and (3) the gallery set affect the re-ID accuracy?

5.1. How Do Viewpoint Distributions in the Training Set Affect Feature Learning?

Experiment design. First, the initial datasets are oracle state containing all viewpoints of training and testing identities, *i.e.*, 36 images of each identity under one camera. We remove some viewpoints selectively from the training set to analyze the influence of missing viewpoints. For comparison, we also randomly remove the same amount of training data for each identity as the benchmark. Specifically, the experimental settings of removing viewpoint on the training set are as follows. (1) *Control group (CG)*: randomly selecting 3/4, 2/4, 1/4 of images for each identity. This experiment is the benchmark of reducing training data. Figure 4 shows the two settings of removing viewpoints. (2) *Control group* (CG*)*: randomly knocking out 3/4, 2/4, 1/4 of viewpoints from 36 for all identities. (3) *Experimental group (EG)*: selectively deleting **continuous** viewpoints (1/4, 2/4, 3/4 from 36 viewpoints) of each identity during training. In this group, the selected continuous viewpoints refer to left, front, right and back sides of the person shown in Fig. 3. Note that, all the above setting has the same number of training images, and the viewpoint of the testing set is uniformly distributed. CG* are the averaged results from repeating the experiment 5 times.

Result analysis. Table 3 shows the experimental results of training on 3/4, 2/4 and 1/4 of the training set. Compared with Oracle, the mAP and R1 of CG are similar or slightly reduced because CG still covers all kinds of viewpoint to train PCB, so the model still can learn enough information from the various viewpoint. After deleting some specific viewpoints in CG*, the decline of results becomes noticeable compared with CG, *e.g.*, the results of 1/4 CG* fall 1.0% - 1.4% relative to CG. By contrast, the results are reduced by a large margin for all the four datasets in EG (*e.g.*, decreasing 1% - 8% of 1/4 EG on PersonX₁₂). It reveals that continuous viewpoints, such as left, back *etc.*, contain different details of body information, so the lack of one side will reduce the information learned by the model. Accordingly, the identifiability of the system is influenced. Furthermore, the discrepancies gradually increase with the decreasing of training data. The detailed comparison of CG, CG* and EG of the PersonX₄₅ and PersonX₄₆ datasets are shown in Fig. 5, and the results are from models trained on different numbers of viewpoints. It is evident, the drop of mAP in EG is more noticeable than CG and CG*, so honk-

#	Group	Viewpoint / Direction	Img#	PersonX ₁₂		PersonX ₁₃		PersonX ₄₅		PersonX ₄₆		Market-1203			
				mAP	R1	mAP	R1	mAP	R1	mAP	R1	Img#	mAP	R1	
1	Oracle	[0°, 350°]	36	97.8	99.6	97.6	99.4	97.7	99.8	96.8	99.2	1-8	77.8	81.4	
	CG	[0°, 350°]	27	97.8	99.6	97.2	99.5	97.6	99.9	96.8	98.8	1-6	72.8	75.9	
	CG*	reserve 27 angles	27	97.7	99.7	97.2	99.5	97.4	99.9	96.4	98.8	1-6*	69.0	73.3	
	EG	delete left	27	97.4	99.6	97.1	99.4	96.9	99.9	96.2	98.6	1-6*	66.6	69.4	
	3/4	EG	delete front	27	97.2	99.6	96.7	99.5	96.6	99.9	96.1	98.9	1-6*	62.1	65.4
	EG	delete right	27	97.5	99.5	97.3	99.2	97.3	99.9	96.4	98.8	1-6*	64.0	97.8	
2/4	EG	delete back	27	97.1	99.5	96.8	99.4	96.7	100	96.1	98.6	1-6*	59.0	62.6	
	CG	[0°, 350°]	18	97.6	99.6	97.0	99.4	97.0	99.9	96.3	98.7	1-4	50.2	53.9	
	CG*	reserve 18 angles	18	97.3	99.6	96.8	99.3	96.8	99.8	96.1	98.8	1-4*	51.3	55.1	
	EG	left+right	18	96.2	99.5	95.7	99.4	95.5	99.9	95.3	98.5	1-4*	44.4	47.9	
	EG	front+back	18	95.4	99.5	94.5	99.2	94.8	99.6	94.2	98.1	1-4*	42.2	45.2	
	EG	front+right (left)	18	96.4	99.5	96.0	99.2	95.9	99.8	95.1	98.2	1-4*	41.0	45.4	
1/4	EG	back+right (left)	18	96.4	99.6	95.8	99.3	95.4	99.8	95.0	98.4	1-4*	45.0	45.7	
	CG	[0°, 350°]	9	97.1	99.6	96.3	99.4	96.5	99.6	95.3	98.1	1-2	-	-	
	CG*	reserve 9 angles	9	95.7	99.5	95.1	99.2	95.1	99.6	94.3	98.1	1-2*	-	-	
	EG	left	9	94.7	99.6	93.7	99.1	93.9	99.6	93.2	98.1	1-2*	-	-	
	EG	front	9	87.7	99.4	86.5	98.8	87.0	99.5	86.6	97.4	1-2*	-	-	
	EG	right	9	94.3	99.5	93.6	95.8	93.7	99.7	93.1	97.9	1-2*	-	-	
EG	back	9	88.1	99.4	85.9	98.6	87.8	99.3	87.4	96.3	1-2*	-	-		

Table 3. Performance using different viewpoints in the training set. “CG” and “EG” denote the control group and experiment group, respectively. #1 Oracle means all 36 viewpoints are contained by training data. 3/4, 1/2 and 1/4 denote the ratio of used training data as a fraction of the Oracle training set. “3/4 CG” means 3/4 of the training images of each identity are randomly selected, so the whole training data still contains all 36 viewpoints. “3/4 CG*” means the training set contains all the identities but only 27 viewpoints. “3/4 EG” means deleting either the left, front, right or back viewpoints (9 continuous viewpoints) for each identity. “Viewpoint / Direction” shows the viewpoints contained in the training set. “Img#” is the number of training images for each identity.

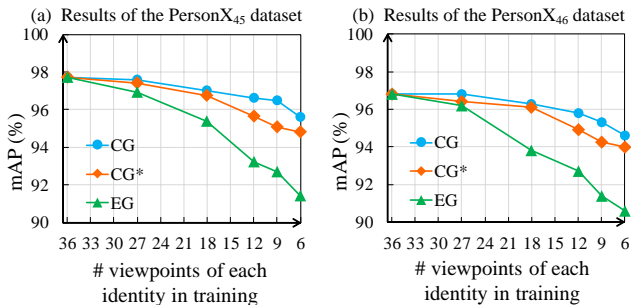


Figure 5. Comparison of results from experimental and control groups on PersonX₄₅ (a) and PersonX₄₆ (b). The horizontal axis is the ratio of training data and the vertical axis is the mAP.

ing out continuous viewpoint will bring more influence for training compared to deleting the same amount of data or discontinuous viewpoint.

On the other hand, the downtrend of “delete front” and “delete back” is more apparent compared with “delete left” and “delete right” (0.2% - 0.5% of mAP) in 3/4 EG. There are two possible reasons. (1) Flipping the left viewpoint can often obtain the right viewpoint, so deleting left or right has the lesser loss than removing “front” or “back”. (2) Because the front and back sides contain more information than left or right sides, the missing front and back bring more influence for the amount of information learned by the model than the other two sides. When training the model on 1/2 of the 36 viewpoints, the results of “front + back” (shadowed in Table 3) decrease by 0.8%-1.5% in mAP compared with training with other viewpoints. Probably because mod-

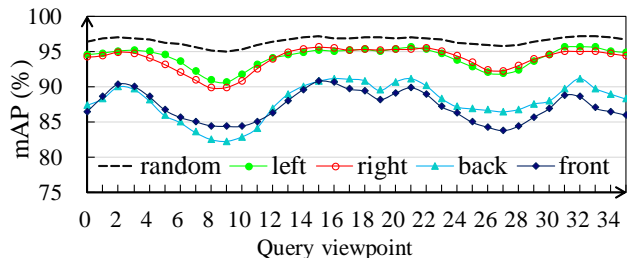


Figure 6. Evaluation of the model trained on the left, front, right and back viewpoints, respectively, when the viewpoints of all queries are same and changed from 0° - 350°. Here, the viewpoint is uniformly distributed in the gallery.

els trained on left or right viewpoint can learn better of the color, outfit (e.g., long or short sleeve, pants, shorts) etc. general information of pedestrian, but models learned from front or back viewpoint tend to capture more detail information of the person, such as prints of clothes, face. Therefore, for the retrieval image is of the left or right viewpoint that does not contain too much detail information, the model trained on “front+back” viewpoint cannot work well. These discussions can also be proved by results of 1/4 EG. The mAP of the model train on left or right viewpoint is almost 6% - 9% higher than learning from the viewpoint from front /back.

To provide detail performance of these four models (trained on the viewpoint of left, right, front and back), we show their mAP when setting all query images to a single viewpoint in Fig. 6. Obviously, taking any viewpoint as the

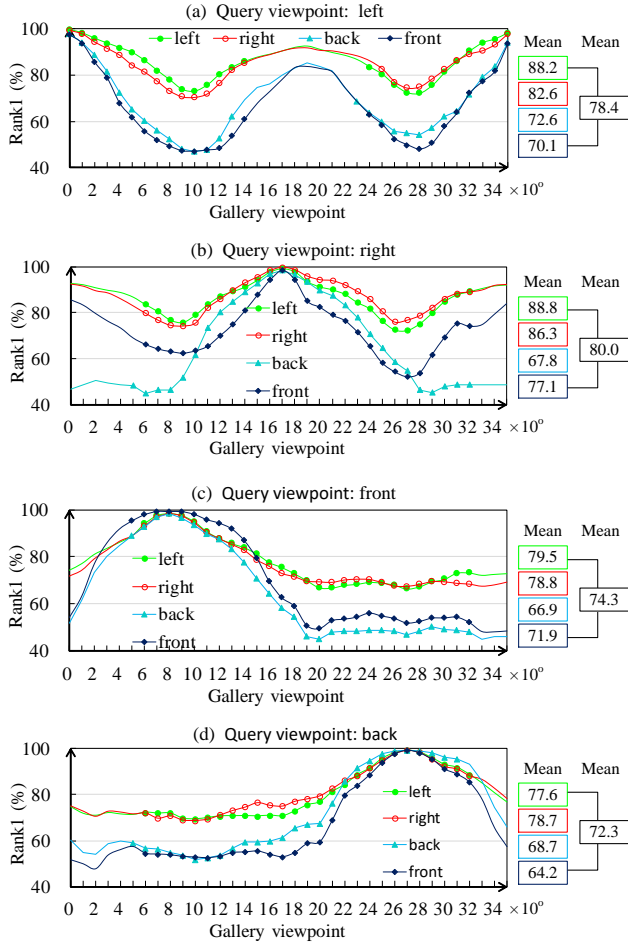


Figure 7. Investigation into query viewpoint. The query viewpoint of every identity is set to left (0°), right (180°), front (90°) and back (270°) in (a) - (d), respectively. In each figure, the horizontal axis represents setting the gallery viewpoint from (0°) to (350°) separately. The results are testing on PersonX₄₅ by the 4 models of EG 1/4 in Table 3. Mean is the average of 27 marked points in each figure (removing the double positive effect of right or left).

query viewpoint, the models trained on the viewpoint of left / right performs favorably against the models learned from viewpoint of front / back. Meanwhile, the same experiment is conducted on the real dataset Market-1203. The decreasing tendency of results changes is consistent with the results changes of synthetic datasets on Oracle, CG, CG* and EG.

Subsection conclusions

- Missing viewpoint compromises training.
- Missing continuous viewpoints are more detrimental than missing randomly viewpoints.
- When limited training viewpoints are available, models can be better trained when left / right viewpoints are in training set than front / back viewpoints.

5.2. How Does Query Viewpoint Affect Retrieval?

Experiment design. We quantify how query viewpoint influences the system. Based on the above training models, we modify the evaluating rules to see the effect of viewpoint during testing.

Specifically, the viewpoint of probe images is set to the **left** viewpoint of person (0°), **front** viewpoint of person (90°), **right** viewpoint (180°) and **back** viewpoint (270°), respectively. During retrieval, the true match is set to the image that contains the same person and viewpoint of the person is $0^\circ - 350^\circ$, separately.

Result analysis. Figure 7 shows the results of using these query and gallery images to test the four models that are trained by the left, right, front, back orientations (see Fig. 3 for the definition of the four orientations), respectively. The consistent results of four settings are that query image will get the highest results when the viewpoint of the true match is similar to the query viewpoint. For example, the maximum values of Rank1 in (a)-(d) correspond to the gallery viewpoint that is same with the query viewpoint. Meanwhile, it is obvious that the query of left and right viewpoint (a) and (b) has a higher mean of Rank1 than (c) and (d) using the query of front or back viewpoint, e.g., the mean R1 80.0% in (b) query of right viewpoint are bigger than the mean values 74.3% of (c). Because query viewpoint of the left can perform better on both left and right, but query viewpoint of front or back do not have these characters. To reduce the positive influence on query viewpoint of left or right, the R1 of 9 gallery viewpoints of right or left do not be considered when calculating the mean value for fair comparison. In this case, query viewpoint of left and right still have high retrieval results.

Subsection conclusions

- Query viewpoint of left/right generally yields higher re-ID accuracy than front/back viewpoints.

5.3. How Do Viewpoint Distributions in Gallery Affect Retrieval?

Finally, we study how the gallery viewpoint distribution affects the re-ID accuracy. Specifically, the gallery images that have similar viewpoints with the probe will be set as junk during testing.

Experiment design. We denote the viewpoint of probe and gallery as θ_p and θ_g , respectively. In experiment, the experimental groups are as follows. 1) gallery images whose $\theta_g \in [\theta_p \pm 10^\circ]$ are set as junk (i.e., -3 images) 2) gallery images whose $\theta_g \in [\theta_p \pm 40^\circ]$ are set as junk (i.e., -9 images). For comparison, we also set -EG to represent junking the gallery images whose $\theta_g \in [\theta_p + 180 \pm 10^\circ]$, because these images can be considered as having a big distance with the query images. The corresponding control groups are randomly setting the same number of images as junk.

#	Training Data	1 vs all		1 vs -3						1 vs -9					
		Oracle		CG		EG		-EG		CG		EG		-EG	
		mAP	R1	mAP	R1	mAP (↓)	R1 (↓)	mAP	R1	mAP	R1	mAP (↓)	R1 (↓)	mAP	R1
1	PersonX ₄₅	97.7	99.8	97.6	99.8	97.4 (0.3)	99.4 (0.4)	97.7	99.8	97.4	99.8	96.6 (1.1)	98.3 (1.5)	97.8	99.8
2	PersonX ₄₅ 3/4	97.6	99.9	97.5	99.9	97.2 (0.4)	98.9 (1.0)	97.6	99.9	97.3	99.8	96.7 (0.9)	98.4 (1.5)	97.7	99.9
3	PersonX ₄₅ 3/4	97.0	99.9	96.9	99.9	96.5 (0.5)	98.9 (1.0)	97.0	99.9	96.9	99.9	95.5 (1.5)	97.4 (2.5)	97.1	99.9
4	PersonX ₄₅ 1/4	96.5	99.6	96.3	99.6	95.9 (0.6)	98.3 (1.3)	96.4	99.6	96.0	99.4	94.8 (1.7)	96.6 (3.0)	96.4	99.6
5	PersonX ₄₆	96.8	99.2	96.7	99.1	96.4 (0.4)	98.2 (1.0)	96.8	99.2	96.4	99.0	95.5 (1.3)	97.1 (2.1)	96.8	99.2
6	PersonX ₄₅ 3/4	96.8	98.8	96.7	98.8	96.4 (0.4)	98.1 (0.7)	96.8	98.8	96.4	98.7	95.5 (1.3)	96.7 (2.1)	96.8	98.8
7	PersonX ₄₆ 2/4	96.3	98.7	96.2	98.7	95.8 (0.5)	97.1 (1.6)	96.3	98.7	95.8	98.5	94.8 (1.5)	95.8 (2.9)	96.3	98.7
8	PersonX ₄₆ 1/4	95.3	98.1	95.1	98.1	94.6 (0.7)	96.6 (1.5)	95.1	98.1	95.2	98.1	93.4 (1.9)	94.9 (3.2)	94.7	97.8
9	PersonX ₄₆ -lr	92.6	96.6	92.4	96.4	91.8 (0.8)	95.9 (0.7)	92.6	96.6	91.7	96.1	90.2 (2.4)	94.3 (2.3)	92.7	96.6
10	PersonX ₄₆ -lr 3/4	92.5	96.0	92.2	95.7	91.7 (0.8)	95.3 (0.7)	92.4	96.0	91.6	95.9	90.0 (2.5)	94.0 (2.0)	92.5	96.0
11	PersonX ₄₆ -lr 2/4	91.7	95.7	91.4	95.6	90.8 (0.9)	94.6 (1.1)	91.6	95.6	90.8	95.4	89.0 (2.7)	93.4 (2.3)	91.7	95.6
12	PersonX ₄₆ -lr 1/4	90.6	95.6	90.2	95.4	89.6 (1.0)	94.3 (1.3)	90.5	95.6	89.5	95.0	87.5 (3.7)	92.7 (2.9)	90.6	95.6
#	Real data	1 vs all		1 vs -3						1 vs -5					
13	Market-1203	77.8	81.4	77.2	79.4	74.7 (3.1)	74.4 (7.0)	77.2	79.4	79.3	79.7	74.1 (3.7)	71.0 (10.4)	83.1	83.0
14	Market-1203 3/4	72.8	75.9	71.6	73.0	68.8 (4.0)	67.9 (8.0)	76.3	76.4	71.5	68.6	68.5 (4.3)	64.9 (11.0)	80.3	79.3
15	Market-1203 2/4	50.2	53.9	48.8	50.0	44.7 (5.5)	43.5 (10.4)	56.3	55.7	48.7	42.7	44.5 (5.7)	41.1 (12.8)	62.3	60.1

Table 4. Evaluation of viewpoint during testing. 1 vs all means database containing 36 viewpoints of each identities. For EG, 1 vs -3 means 3 gallery images that have same id with probe and $\theta_g \in [\theta_p \pm 10]$, are defined as junk during testing. For -EG, it means $\theta_g \in [(\theta_p + 180) \pm 10]$ are defined as junk during testing, *i.e.*, the most different gallery images are defined as junk. CG represents randomly select the same number of images are taken as junk. 1 vs -9 corresponds to take gallery images with $\theta_g \in [\theta_p \pm 40]$ ($\theta_g \in [(\theta_p + 180) \pm 40]$) as junk. (↓) represents the discrepancy of result compared with the result in column of Oracle.

Since Market-1203 only contains 8 kinds of angles, -3 and -5 means junking the images with the viewpoint similar to the probe viewpoint, *e.g.*, -3 refers to removing the exact viewpoint that is same with probe viewpoint, and it is the previous and next viewpoints.

Result analysis. Experimental results in Table 4 show that randomly setting 3 or 9 gallery images of each person as junk, *i.e.*, control group (CG), has a negligible effect on the results. Meanwhile, the results approximately keep unchanged in -EG when junking 3 images, but there is a rising of most of the result in “1 vs -9” due to the removing of hard retrieval gallery images and the narrowing of the database. For example, in #1 of Table 4, compared to the Oracle results 97.7% (mAP) and 99.8% (R1), the results of CG (1 vs -9) 97.4% (mAP) and 99.8% (R1) has some small changes. In -EG, the mAP of 97.8% rises by 0.1%. On the contrary, the results of experimental groups (EG) have obvious decreases, especially on R1. For instance, in #1 (1 vs -9), the results of EG are 96.6% (mAP) and 98.3% (R1), *i.e.*, there are decreases of 1.1% on mAP and 1.5% on R1. Therefore, the results of the well-learned model will be effected when the viewpoint of gallery images is not similar to the query image. The consistent changes of results can also be summarized on the real dataset Market-1203. In row #13, there are a decrease of 3.1% - 3.7% on mAP and a decrease of 7% - 10% on R1. Meanwhile, there is a phenomenon that R1 has more manifest changes than mAP. One possible reason is that similar viewpoints are ranked early rather than the image from the same person, when junking the true matches with similar viewpoints in the gallery. On the other hand, the reduction of mAP becomes more obvious with the environment becoming hard.

For example, the decline in results of the PersonX₄₆-lr (in row #9) dataset is approximately twice as big as the decline in results of the PersonX₄₆ dataset (in row #5).

Subsection conclusions

- Sometimes true matches whose viewpoints are dissimilar to the query are harder to be retrieved than *false matches with a similar viewpoint*.
- The above problem gets more severe when the environment is less ideal, *e.g.*, complex background, extreme illumination, and low resolution.

6. Conclusion

This paper makes a step from engineering new technologies to science new discoveries. We make two contributions to the community. First, we build a synthetic data engine PersonX that can generate images under controllable cameras and environments. Subsets of PersonX are shown to be indicative of the real world. Second, based on PersonX, we conduct comprehensive experiment to quantitatively assess the influence of pedestrian viewpoint on person re-ID accuracy. Interesting and constructive insights are derived, *e.g.*, it is better to use a query image capturing the side view of a person. In the future, visual factors such as illumination and background will be studied with this new engine.

References

- [1] S. Bak, P. Carr, and J.-F. Lalonde. Domain adaptation through synthesis for unsupervised person re-identification. *arXiv preprint arXiv:1804.10094*, 2018. 2, 4

- [2] S. Bak, S. Zaidenberg, B. Boulay, and F. Bremond. Improving person re-identification by viewpoint cues. In *AVSS*, pages 175–180, 2014. 2
- [3] I. B. Barbosa, M. Cristani, B. Caputo, A. Rognhaugen, and T. Theoharis. Looking beyond appearances: Synthetic training data for deep cnns in re-identification. *Computer Vision and Image Understanding*, 167:50–62, 2018. 2, 4
- [4] L. Bazzani, M. Cristani, A. Perina, and V. Murino. Multiple-shot person re-identification by chromatic and epitomic analyses. *Pattern Recognition Letters*, 33(7):898–903, 2012. 2
- [5] D. Chen, S. Zhang, W. Ouyang, J. Yang, and Y. Tai. Person search via a mask-guided two-stream cnn model. In *ECCV*, 2018. 2
- [6] Y.-J. Cho and K.-J. Yoon. Improving person re-identification via pose-aware multi-shot matching. In *CVPR*, pages 1354–1362, 2016. 2
- [7] M. Farenzena, L. Bazzani, A. Perina, V. Murino, and M. Cristani. Person re-identification by symmetry-driven accumulation of local features. In *CVPR*, 2010. 2
- [8] A. Gaidon, Q. Wang, Y. Cabon, and E. Vig. Virtual worlds as proxy for multi-object tracking analysis. In *CVPR*, 2016. 2
- [9] D. Gray and H. Tao. Viewpoint invariant pedestrian recognition with an ensemble of localized features. In *ECCV*, 2008. 2
- [10] A. Hermans, L. Beyer, and B. Leibe. In defense of the triplet loss for person re-identification. *arXiv preprint arXiv:1703.07737*, 2017. 4
- [11] X.-Y. Jing, X. Zhu, F. Wu, X. You, Q. Liu, D. Yue, R. Hu, and B. Xu. Super-resolution person re-identification with semi-coupled low-rank discriminant dictionary learning. In *CVPR*, 2015. 2
- [12] S. Karanam, Y. Li, and R. J. Radke. Person re-identification with discriminatively trained viewpoint invariant dictionaries. In *ICCV*, 2015. 2
- [13] W. Li, R. Zhao, T. Xiao, and X. Wang. Deepreid: Deep filter pairing neural network for person re-identification. In *CVPR*, 2014. 4
- [14] X. Li, K. Wang, Y. Tian, L. Yan, F. Deng, and F.-Y. Wang. The paralleleye dataset: A large collection of virtual images for traffic vision research. *IEEE Transactions on Intelligent Transportation Systems*, (99):1–13, 2018. 2
- [15] X. Li, W.-S. Zheng, X. Wang, T. Xiang, and S. Gong. Multi-scale learning for low-resolution person re-identification. In *ICCV*, 2015. 2
- [16] J. Riccitiello. John riccitiello sets out to identify the engine of growth for unity technologies (interview). *VentureBeat. Interview with Dean Takahashi*. Retrieved January, 18, 2015. 2
- [17] E. Ristani, F. Solera, R. Zou, R. Cucchiara, and C. Tomasi. Performance measures and a data set for multi-target, multi-camera tracking. In *ECCV*, pages 17–35, 2016. 4
- [18] S. Sankaranarayanan, Y. Balaji, A. Jain, S. N. Lim, and R. Chellappa. Learning from synthetic data: Addressing domain shift for semantic segmentation. In *CVPR*, 2018. 2
- [19] M. S. Sarfraz, A. Schumann, A. Eberle, and R. Stiefelwagen. A pose-sensitive embedding for person re-identification with expanded cross neighborhood re-ranking. In *CVPR*, 2018. 2
- [20] C. Song, Y. Huang, W. Ouyang, and L. Wang. Mask-guided contrastive attention model for person re-identification. In *CVPR*, 2018. 2
- [21] C. Su, J. Li, S. Zhang, J. Xing, W. Gao, and Q. Tian. Pose-driven deep convolutional model for person re-identification. In *ICCV*, 2017. 2
- [22] Y. Sun, L. Zheng, Y. Yang, Q. Tian, and S. Wang. Beyond part models: Person retrieval with refined part pooling (and a strong convolutional baseline). In *ECCV*, 2018. 4, 5
- [23] M. Tian, S. Yi, H. Li, S. Li, X. Zhang, J. Shi, J. Yan, and X. Wang. Eliminating background-bias for robust person re-identification. In *CVPR*, 2018. 2
- [24] Y. Wang, L. Wang, Y. You, X. Zou, V. Chen, S. Li, G. Huang, B. Hariharan, and K. Q. Weinberger. Resource aware person re-identification across multiple resolutions. In *CVPR*, 2018. 2
- [25] Z. Wu, Y. Li, and R. J. Radke. Viewpoint invariant human re-identification in camera networks using pose priors and subject-discriminative features. *IEEE transactions on pattern analysis and machine intelligence*, 37(5):1095–1108, 2015. 2
- [26] T. Xiao, S. Li, B. Wang, L. Lin, and X. Wang. Joint detection and identification feature learning for person search. In *CVPR*, 2017. 2
- [27] K. Zheng, X. Fan, Y. Lin, H. Guo, H. Yu, D. Guo, and S. Wang. Learning view-invariant features for person identification in temporally synchronized videos taken by wearable cameras. In *ICCV*, 2017. 2
- [28] L. Zheng, Z. Bie, Y. Sun, J. Wang, C. Su, S. Wang, and Q. Tian. Mars: A video benchmark for large-scale person re-identification. In *European Conference on Computer Vision*, 2016. 4
- [29] L. Zheng, Y. Huang, H. Lu, and Y. Yang. Pose invariant embedding for deep person re-identification. *arXiv preprint arXiv:1701.07732*, 2017. 2
- [30] L. Zheng, L. Shen, L. Tian, S. Wang, J. Wang, and Q. Tian. Scalable person re-identification: A benchmark. In *ICCV*, 2015. 2, 4, 5
- [31] Z. Zheng, L. Zheng, and Y. Yang. Unlabeled samples generated by gan improve the person re-identification baseline in vitro. In *ICCV*, 2017. 2, 5
- [32] Z. Zhong, L. Zheng, Z. Zheng, S. Li, and Y. Yang. Camera style adaptation for person re-identification. In *CVPR*, 2018. 4